INORGANIC CHEMISTRY FRONTIERS

RESEARCH ARTICLE

View Article Online
View Journal | View Issue

Cite this: *Inorg. Chem. Front.*, 2024, **11**, 2384

Three in one: a cadmium bismuth vanadate NLO crystal exhibiting a large second-harmonic generation response and enhanced birefringence†

Shuya Liu,[a] Conggang Li, *[a,c] Jinmiao Jiao,[a] Yuheng She,[a] Tinghui Zhang,[a] Dianxing Ju,[b] Ning Ye,[a] Zhanggui Hu*[a] and Yicheng Wu[a]

Received 27th January 2024,
Accepted 9th March 2024

DOI: 10.1039/d4qi00261j

rsc.li/frontiers-inorganic

Inorganic nonlinear optical (NLO) crystals have attracted considerable attention due to their profound applications in laser technology. In this study, we present the synthesis of a novel cadmium bismuth vanadate crystal, Cd_2BiVO_6, through a spontaneous crystallization approach. The title compound, containing d^0 V^{5+}, d^{10} Cd^{2+}, and stereo-active lone pair effect (Bi^{3+}) cations, crystallizes in the non-centrosymmetric orthorhombic space group $Cmc2_1$ (No. 36), characterized by isolated $[VO_4]$ tetrahedra, twisted 1D chains $[Bi_2O_8]_\infty$ and pseudo-2D layers $[Cd_6O_{30}]_\infty$. Remarkably, the structural characteristics endow Cd_2BiVO_6 with a strong second harmonic generation response of around 1.4 × KDP (25–53 μm), and a notably enlarged birefringence of 0.127 at 1064 nm, exceeding 6 times that of the vanadate NLO crystal Li_3VO_4 (~0.021). Thermophysical analyses unveil its exceptional thermal stability up to 900 °C with a commendable congruent nature. Moreover, Cd_2BiVO_6 features a wide transparency range, with the UV and IR cutoff absorption edges observed at 0.395 and ~5.8 μm, respectively. Besides, the observed optical characteristics associated with the microstructure of Cd_2BiVO_6 are explained through electronic structure calculations.

Introduction

Inorganic vanadate materials hold prominence in electrochemical energy storage, catalysts, electronic devices, and laser science as they exhibit good ionic conductivity, catalytic abilities, electrical properties, and nonlinear optical (NLO) properties, rendering them a subject of sustained interest.[1–4] Structurally, vanadate exhibits a variety of coordination geometries, including $[VO_4]$ tetrahedra, $[VO_5]$ pyramids, and $[VO_6]$ octahedra, capable of forming frameworks spanning zero-dimensional (0D) to three-dimensional (3D) ones.[5–7] It is worth noting that the combined characteristics and spatial arrangement of these structural primitives influence certain intrinsic properties associated with the structure, particularly as exemplified in the realm of NLO crystals.[8–11] Moreover, the d^0 transition metal V^{5+} is susceptible to second-order Jahn–Teller (SOJT) effect distortion, which contributes significantly to second order polarizability and optical anisotropy.[12–14] These intricate structural chemistry and distortion characteristics enable the production of favorable second harmonic generation (SHG) activity and birefringence. Accordingly, vanadate-based materials have emerged as a promising class of candidates for exploring NLO crystals.

In recent years, a multitude of vanadate-based NLO materials have been synthesized. For example, the alkali metal vanadates, including Li_3VO_4, $Cs_2V_3O_8$, $A_3V_5O_{14}$ (A = K, Rb), A_2LiVO_4 (A = Rb, Cs), and $Cs_4V_8O_{22}$, are characterized by favorable NLO properties because of the stable covalent interactions within the V–O bonds.[15–19] Notably, $Cs_4V_8O_{22}$ demonstrates a strong phase-matchable SHG intensity of 12.0 × KDP@1064 nm, largely attributed to the $[V_4O_{11}]_\infty$ layers composed of $[VO_4]$ and $[VO_5]$ polyhedra. The borate vanadates $K_2SrVB_5O_{12}$ and $Na_3VO_2B_6O_{11}$, comprising $[VO_4]$ tetrahedra and $[BO_3]$ triangles, show SHG intensities comparable to those of KDP.[20,21] The rare earth vanadates $Ca_9RE(VO_4)_7$ (RE = La, Yb, Y) crystallize into a polar space group and exhibit favorable SHG activities of 4 × KDP.[22] Additionally, the main group d^0 transition metal vanadates $SrM_2V_2O_{11}$ (M = Nb, Ta) feature unique $[M_2V_2O_{11}]^{2-}$ anionic layers, resulting in high SHG

[a]*Tianjin Key Laboratory of Functional Crystal Materials, Institute of Functional Crystal, Tianjin University of Technology, Tianjin 300384, China. E-mail: cgli@email.tjut.edu.cn, hu@mail.ipc.ac.cn*
[b]*College of Materials Science and Engineering, Qingdao University of Science and Technology, Qingdao 266042, P.R. China*
[c]*State Key Laboratory of Crystal Materials, Shandong University, Jinan, 250100, China*

†Electronic supplementary information (ESI) available: Additional crystallographic data, PXRD and EDS analyses, powder presentation and experimental birefringence of Cd_2BiVO_6. CCDC 2326701. For ESI and crystallographic data in CIF or other electronic format see DOI: https://doi.org/10.1039/d4qi00261j

efficiencies.[23] These investigations predominantly introduce one or two types of NLO-active units within a single compound.[24] However, the incorporation of three distinct NLO-active chromophores in one compound is rarely studied. To date, only one NLO crystal, namely $Cd_4V_2Te_3O_{15}$, containing a d^0 transition metal cation, a stereochemically active lone-pair cation, and a polar displacement d^{10} cation, has been reported in the vanadate family.[25] Hence, the investigation of vanadates with multiple chromophores holds great significance not only for the advancement of novel NLO crystals but also for unveiling the interplay between the structures and properties of these materials.

In this study, we devoted particular attention to the cadmium bismuth vanadate Cd_2BiVO_6 (CBVO), due to the presence of d^0–d^{10} stereochemically active lone-pair (SCALP)-effect cations, serving as fundamental building blocks. The d^0 transition metal cation V^{5+}, the SCALP cation Bi^{3+}, and the d^{10} cation Cd^{2+} with polar displacement demonstrate flexible asymmetric coordination modes, thereby enhancing second-order microscopic polarizability and structural anisotropy.[26,27] Moreover, the heavy element attributes of these cations effectively extend the infrared transmittance range. In 2000, Sleight *et al.* evaluated the cell parameters of CBVO solely using powder X-ray diffraction.[28] Nevertheless, the structural refinement, crystal growth, optical characteristics and the structure–performance correlation of CBVO have remained unexplored. Inspired by this, we synthesized CBVO crystals *via* spontaneous crystallization methods for the first time. Single crystal X-ray diffraction analysis of CBVO was performed, revealing a unique 3D structural framework composed of isolated $[VO_4]$ tetrahedra, twisted 1D chains $[Bi_2O_8]_\infty$ and pseudo-2D layers $[Cd_6O_{30}]_\infty$. The thermal stability and congruent melting nature of the title compound were evaluated. Moreover, optical characterization demonstrated that CBVO exhibits a strong SHG response, a notably large birefringence, and a wide transmission range, indicating its good potential as NLO crystals. Besides, the origin of the optical performances for CBVO was also elucidated through electronic structure calculations.

Experimental section

Materials preparation

The reagents, namely CdO, Bi_2O_3, and V_2O_5 of analytical pure grade, were procured commercially. The CBVO polycrystalline compound was synthesized using a high-temperature solid-state reaction method. The reagents CdO, Bi_2O_3 and V_2O_5, with a molar ratio of 4 : 1 : 1 were thoroughly ground in a mortar and subsequently placed into a Pt crucible. The mixture was heated up to 780 °C at a rate of 10 °C min^{-1} in a muffle furnace, followed by sintering for 60 hours, and then cooling to room temperature at a rate of 5 °C min^{-1}. The purity of the resulting compound was verified using powder X-ray diffraction (PXRD) analysis. CBVO single crystals were prepared *via* the spontaneous crystallization technique. The CBVO polycrystalline powder, held in a Pt crucible, was heated to 950 °C, and maintained at this temperature for no less than 24 hours to ensure a uniform melt. The solution was then gradually cooled to 650 °C at a rate of 5–10 °C h^{-1} before being further lowered to room temperature through air-cooling, yielding the crystals of CBVO.

Characterization

PXRD measurements of CBVO were performed at room temperature utilizing a Rigaku SmartLab 9 kW diffractometer (λ = 1.5418 Å). The data were captured within the 2θ range from 10° to 70° with a scanning step size of 0.01° s^{-1}. Single crystal X-ray diffraction data were acquired using a Bruker SMART APEX III CCD diffractometer at 293 (2) K with Mo *K*a radiation (λ = 0.71073 Å) and processed using the SAINT program.[29] The preliminary structural model and atomic positions of CBVO were determined employing the direct method within the SHELXTL system.[30] The structure was scrutinized for potential missing symmetry using the PLATON program.[31] Tables S1 and S2 (ESI†) show the detailed crystallographic data, including atomic coordinates, equivalent isotropic parameters, selected bonds and angles as well as valence calculations. The coexistence and distribution of the Cd, Bi, V, and O elements were detected using a field emission scanning electron microscope (Quanta FEG 250) with an energy dispersive *X*-ray spectroscope. Thermal assessment of CBVO was carried out by employing a NETZSCH STA 449F5 TG/DSC thermal analyzer instrument. Milligram samples were placed in an Al_2O_3 crucible and heated from room temperature to 1000 °C at a rate of 10 °C min^{-1} under a constant nitrogen atmosphere. The UV-Vis-NIR diffuse reflectance spectra of CBVO was executed at room temperature employing a UH4150 spectrophotometer covering a range from 200 to 2000 nm, with barium sulfate utilized as a reference. The optical band gap was estimated using the Kubelka–Munk equation.[32] The infrared spectra of CBVO were characterized using a Nicolet iS50 FT-IR infrared spectrometer at room temperature across a wavelength range of 400–4000 cm^{-1}. The powder second-harmonic generation (SHG) response of CBVO was measured using the Kurtz–Perry approach on a Q-switched Nd : YAG laser (1064 nm).[33] CBVO polycrystalline samples were meticulously ground and sieved into a particle size range of 25–53 μm. Concurrently, the KH_2PO_4 (KDP) samples with the same particle sizes were also prepared as a reference. The birefringence of CBVO was detected using a Nikon Eclipse E200MV POL polarizing microscope with a visible light source and determined by the following criterion:[34] $R = |Ne - No| \times d = \Delta n \times d$, where R, Δn, and T represent the optical path difference, optical birefringence, and the thickness of the crystal, respectively.

Computational methods

To elucidate the electronic structures, we employed density functional theory (DFT) in conjunction with the CASTEP program to conduct atomic-level theoretical computations on CBVO.[35,36] The generalized gradient density approximation with the Perdew–Burke–Ernzerhof (GGA-PBE) functional was implemented throughout the calculations.[37,38] The valence

electron configurations, as elucidated by the norm-conserving pseudopotential (NCP), are as follows: Cd $5s^2$ $4d^{10}$, Bi $6s^2$ $6p^3$ $5d^{10}$, V $3d^3$ $4s^2$, and O $2s^2$ $2p^4$. To ascertain the plane wave number of CBVO, a kinetic energy cutoff of 830 eV was specified, with the numerical integration of the Brillouin zone conducted using a 4 × 3 × 6 Monkhorst–Pack *k*-point.

Results and discussion

Synthesis and thermal properties

The CBVO compounds were experimentally prepared through the conventional ceramic calcination process, employing a suitable mixture of CdO, Bi_2O_3 and V_2O_5 raw materials. As shown in Fig. 1a, the resultant product demonstrates high purity, as evidenced by powder X-ray diffraction (PXRD) patterns, and the experimental observations agree well with those derived from the structural model. The thermal characteristics of CBVO were evaluated through TG/DSC examinations. As illustrated in Fig. 1b, CBVO displays notable thermal stability, as indicated by a single endothermic peak at around 900 °C in the DSC pattern, without a corresponding weight loss in the TG curve. Moreover, as demonstrated in Fig. S1,† no distinct discrepancy is discernible in the PXRD patterns before and after the melting of CBVO, implying its commendable congruent melting feature.

Structural analyses

Owing to the challenging nature of the crystal growth of CBVO, the structural analysis of CBVO has thus far been confined to the powder X-ray diffraction characteristic, rendering its structural data incomplete.[28] Our prior studies demonstrated that the title compound exhibits congruent melting properties. Accordingly, we synthesized the CBVO crystals by melting pure polycrystalline powder and inducing its spontaneous crystallization through programmed slow cooling. Following numerous attempts at crystal growth, small single crystals of CBVO were successfully extracted. Subsequently, we selected well-formed crystals with regular and transparent features for implementing single-crystal X-ray diffraction analyses. Our examinations revealed that CBVO crystallizes in the asymmetric orthorhombic space group, $Cmc2_1$ (No. 36), with the following unit cell parameters: a = 8.6516(16) Å, b = 11.4740(2) Å, c = 5.6533(13) Å and Z = 4 (Table 1). Additional structural information including the atomic coordinates, bond lengths/angles, the equivalent displacement parameters, and valence bond calculations for CBVO is summarized in Tables S1 and S2.† Within the asymmetric unit of CBVO, there exist one distinct Cd site, one distinct Bi site, and one distinct V site. As shown in Fig. 2a, the V^{5+} cation is coordinated to four oxygen atoms, forming irregular [VO_4] tetrahedra with a spread of V–O bond distances varying from 1.693(11) to 1.740(10) Å. The Bi^{3+}

Table 1 Crystallographic data and structural refinement of CBVO

Empirical formula	Cd_2BiVO_6
Formula weight	580.72
Temperature (K)	293(2) K
Wavelength (Å)	0.71073 Å
Crystal system	Orthorhombic
Space group	$Cmc2_1$
a (Å)	8.6516(16)
b (Å)	11.474(2)
c (Å)	5.6533(13)
Volume (Å^3)	561.2(2)
Z	4
ρ_{calcd} (g cm^{-3})	6.873
F (000)	1000
Completeness	100%
R (int)	0.0310
GOF (F^2)	1.129
Final R indices [$F_o^2 > 2\sigma(F_o^2)$][a]	R_1 = 0.0209, wR_2 = 0.0525
R indices (all data)	R_1 = 0.0218, wR_2 = 0.0527
CCDC number	2326701†

[a] $R_1 = \sum||F_o| - |F_c||/\sum|F_o|$; w$R_2 = [\sum w(F_o^2 - F_c^2)^2/\sum w(F_o^2)^2]^{1/2}$.

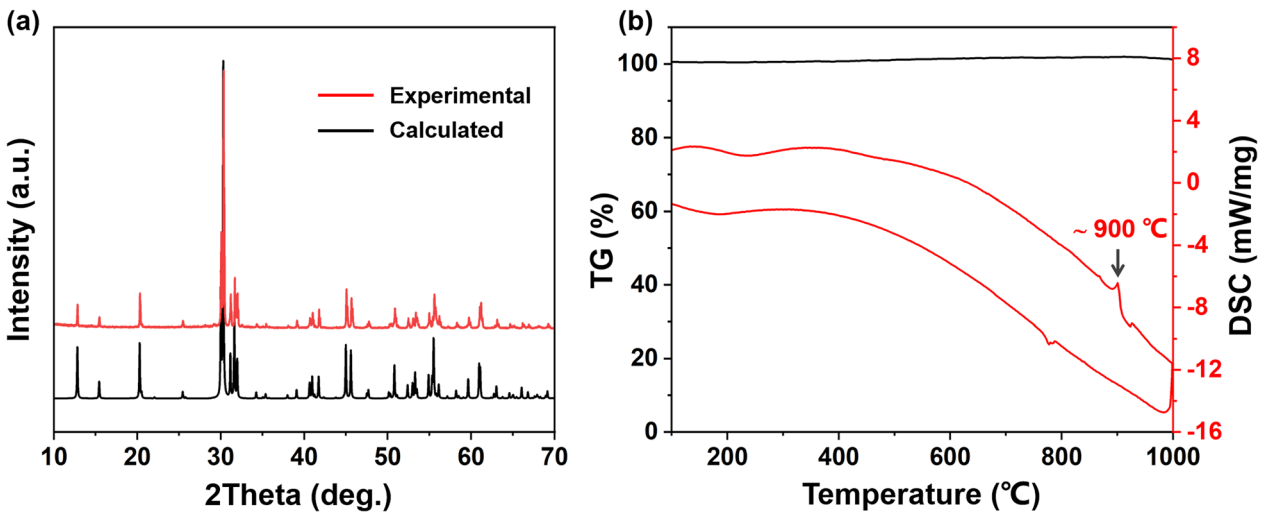

Fig. 1 (a) Experimental and calculated PXRD patterns of CBVO. (b) Presentation of DSC-TG analysis of CBVO.

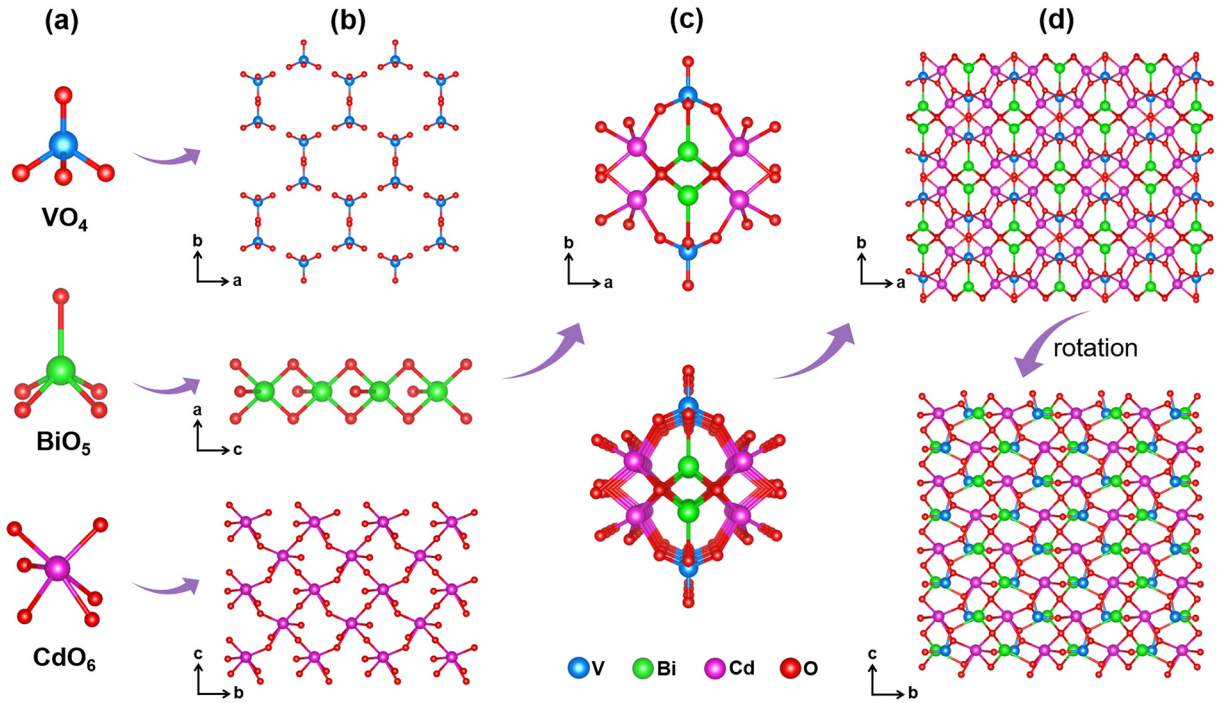

Fig. 2 Presentation of the structure of CBVO. (a) Functional building units [VO_4], [BiO_5], and [CdO_6]. (b) Antiparallel arrangement of 0D [VO_4] units, a 1D twisted $[Bi_2O_8]_\infty$ chain, and a pseudo-2D layer parallel to the *bc* plane. (c) A $[Bi_2V_2Cd_4O_{27}]$ fragment and a 1D briquette-like $[Bi_2V_2Cd_4O_{27}]_\infty$ channel structure. (d) 3D structural network viewed from the *ab* and *bc* planes, respectively.

cation is connected with five oxygen atoms, resulting in a distortive pyramidal geometry [BiO_5], with the Bi–O bond lengths falling within the range of 2.210(2)–2.616(13) Å. The Cd^{2+} cation is bound to six oxygen atoms, yielding [CdO_6] octahedra, and displaying a spread of Cd–O bond distances ranging from 2.241(18) to 2.405(10) Å. As depicted in Fig. 2b, all [VO_4] tetrahedra exist in isolation distinguished by an antiparallel arrangement, and display zero-dimensional (0D) characteristics. Meanwhile, the neighboring [BiO_5] polyhedra are interconnected *via* edge-sharing, giving rise to a twisted one-dimensional (1D) $[Bi_2O_8]_\infty$ chain that extends infinitely along the *a*-axis. Additionally, the adjacent [CdO_6] polyhedra are bridged by shared oxygen atoms, yielding the formation of a pseudo-two-dimensional (2D) layer parallel to the *bc* plane. As shown in Fig. 2c, the functional building motifs [VO_4], [BiO_5] and [CdO_6] are interlinked to form a $[Bi_2V_2Cd_4O_{27}]$ fragment, which further extends indefinitely along the *c*-axis, yielding a 1D briquette-like $[Bi_2V_2Cd_4O_{27}]_\infty$ channel structure. The channel-like structure continues indefinitely along the *a* and *b*-axes, contributing to the 3D structural framework of CBVO, as presented in Fig. 2d.

Furthermore, bond-valence sum (BVS) calculations were performed, yielding the anticipated valence states of CBVO (Table S2†). EDS measurements, as illustrated in Fig. S2,† were also performed to ascertain the elemental distribution of CBVO, resulting in an average Cd/Bi/V/O atomic ratio of 2.07 : 1.06 : 1.0 : 5.9, in line with that derived from single-crystal XRD data. Clearly, these aforementioned analyses further confirm the validity of the observed structure of the CBVO crystal.

Second-harmonic generation measurements

Given the absence of a symmetrical center in the structure of the title compound, the SHG behavior of a polycrystalline powder of CBVO was investigated utilizing a laser with a wavelength of 1064 nm, with KDP serving as a reference material. It is noteworthy that the dispersion of the CBVO polycrystalline compound exhibits considerable strength, rendering it a great challenge to maintain its compactness and shape. This presents significant hurdles in the preparation of SHG test samples with various particle size ranges. As a result, for the purposes of this SHG test experiment, our preparation was limited to a specific particle size range for the title compound. As shown in Fig. 3a, CBVO demonstrates a strong powder SHG activity, approximately 1.4 times that of the KDP within the 25–53 μm particle size range. This substantiates the non-central symmetry of the CBVO structure, signifying its characterization as an NLO crystal.

Spectroscopy characterization

The UV-Vis-NIR diffuse reflectance spectra of CBVO polycrystalline samples are displayed in Fig. 3b, revealing an extension of the UV absorption cut-off edge to approximately 395 nm. Analysis using the Kubelka–Munk equation yielded a corresponding band gap of 2.78 eV, which aligns with the observed light-yellow color (Fig. S3†). Furthermore, the IR spectrum,

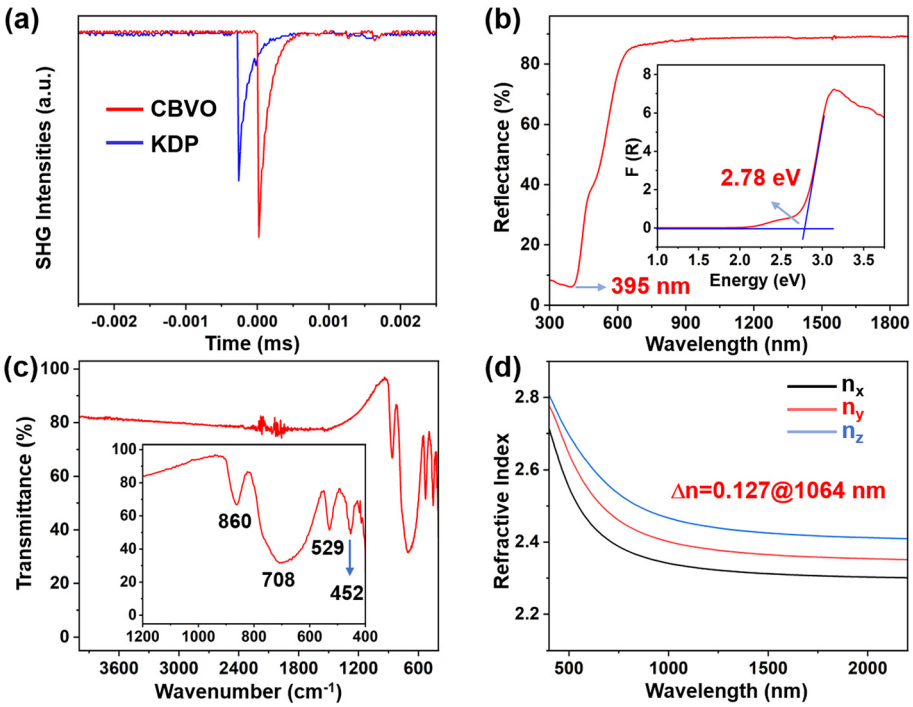

Fig. 3 Optical characterization. (a) SHG intensity of the CBVO compound compared to that of the KDP reference. (b) UV-vis-NIR diffuse reflectance spectra and band gap of CBVO. (c) IR spectrum of CBVO. (d) Calculated refractive indices of CBVO.

ranging from 4000 to 400 cm^{-1}, was employed to elucidate its optical transmission characteristics. Clearly, Fig. 3c shows negligible absorption across a broad region from 4000 to 860 cm^{-1}, which implies an IR cut-off edge of approximately 5.8 μm determined by the two-phonon approximation.[39] Taking into account the potential variation in the IR cutoff edge resulting from multiphonon absorption in powder and crystal measurements, we made adjustments by eliminating 50% of the data. The optical features indicate that CBVO possesses a broad transmission range encompassing the crucial 3–5 μm atmospheric window, exceeding that of the commonly used vanadate crystal YVO_4.[40,41] These attributes highlight the potential of CBVO for applications as NLO crystals in a favorable wavelength range. Specifically, the characteristic absorption peaks at 860 and 708 cm^{-1} primarily arise from the stretching vibrations of $[VO_4]$ tetrahedra, while that observed at 452 cm^{-1} stems from the V–O–V vibrations. Additionally, the absorption bands located at around 529 cm^{-1} are attributed to the Bi—O vibrations in CBVO. As expected, these spectral analysis results align with the structural characteristics and are consistent with previously reported findings.[42–47]

Birefringence properties

The birefringence of a material can be regarded as a manifestation of its inherent structural anisotropy. We examined the birefringence of the CBVO crystal using a polarizing microscope. Fig. S4a and b† demonstrate the appearance of the CBVO crystal before and after extinction under orthotropic polarized light, respectively. Furthermore, the actual observed microscopic morphology and theoretical morphology of the crystal CBVO are provided in Fig. S4c and d,† respectively. The retardation R and the thickness of the CBVO crystal were found to be 2.475 μm and 19.1 μm, respectively. Accordingly, the birefringence of CBVO was determined to be approximately 0.130 in the visible wavelength range using the equation $R = \Delta n \times d$. Additionally, the theoretical birefringence of CBVO was also revealed based on first principles calculations (Fig. 4a), with a birefringence value of 0.127 @1064 nm, which agrees well with the experimental findings. Notably, this birefringence of CBVO is larger than those of many other vanadate NLO crystals, such as Li_3VO_4 (0.021), $LiCs_2VO_4$ (~0.028), $LiRb_2VO_4$ (~0.025), and $BaV_2O_6{\cdot}H_2O$ (~0.005).[11,48,49] The birefringence properties exhibited by CBVO not only ensure its ability for phase matching, but also signify its potential as a birefringent crystal.

Theoretical calculations

To shed light on the origin of the optical performances of CBVO, an analysis of its band structure and density of states characteristics was performed. As depicted in Fig. 4a, the disparity in location between the bottom of the conduction band and the top of the valence band suggests that CBVO is an indirect semiconductor compound, yielding a band gap value of 2.26 eV. Moreover, the total density of states (TDOS) and the corresponding partial density of states (PDOS) are also shown in Fig. 4b, revealing that the bottom of the conduction band (CB) is predominantly ascribed to the V 3d, Cd 5s, and Bi 6p orbitals, while the top of the valence band (VB) primarily orig-

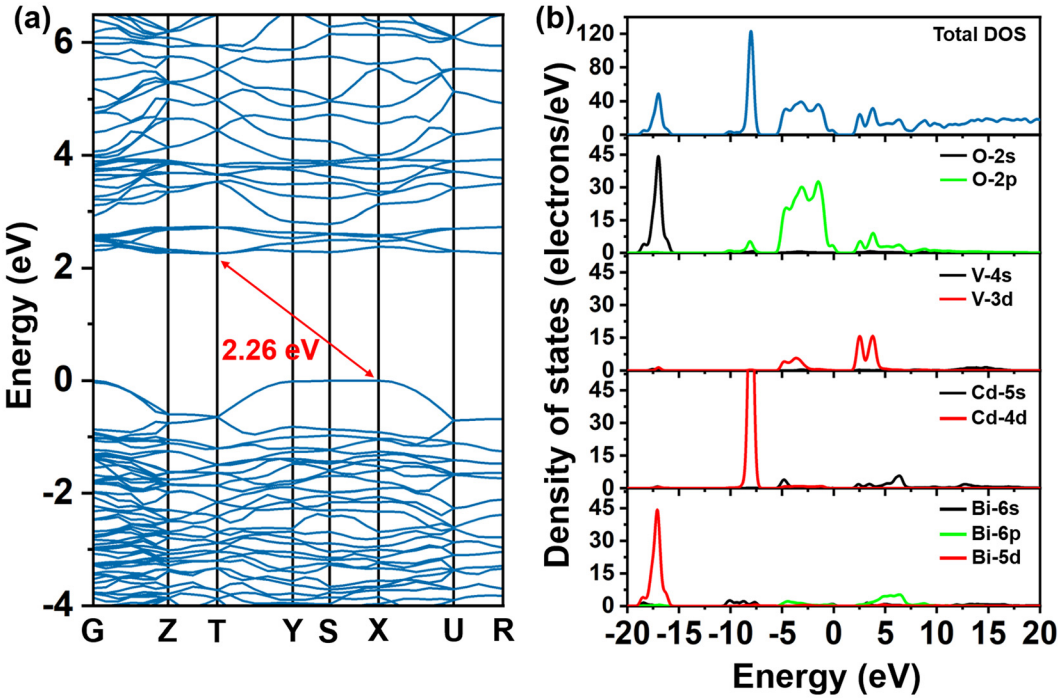

Fig. 4 (a) Band structure of CBVO. (b) Partial and total density of states of CBVO.

inates from the O 2p and V 3d orbitals. The valence bands within the energy range of −15 to −20 eV are composed of the Bi 5d and O 2s orbitals, indicating a negligible impact on the band gaps of CBVO. According to criteria, the optical properties of a material are substantially influenced by its electronic states in close proximity to the forbidden band.[50] Consequently, the NLO activities originate from the synergistic effect of the $[VO_4]$ tetrahedra, $[CdO_6]$ octahedra, and $[BiO_5]$ pyramids of CBVO.

Conclusions

To summarize, the bismuth vanadate bismuth crystal, CBVO, has been successfully extracted *via* modified spontaneous crystallization for the first time. Single-crystal X-ray diffraction unveiled that it features a distinctive 3D structural network comprising 0D $[VO_4]$ groups, 1D $[Bi_2O_8]_\infty$ chains, and pseudo-2D $[Cd_5O_{26}]_\infty$ layers. Thermal assessments indicated that CBVO has high thermal stability with favorable congruent melting behavior. Notably, optical measurements demonstrated that it exhibits strong powder SHG effects, approximately 1.4 times that of the KDP, and achieves a notably large birefringence of 0.127 at 1064 nm. Moreover, the title compound displays an extended transmission window from 0.395 to 5.8 μm, encompassing the significant atmospheric window of 3–5 μm. Additionally, theoretical investigations of CBVO suggested that the observed optical features are primarily governed by the $[VO_4]$ tetrahedra, $[CdO_6]$ octahedra, and $[BiO_5]$ pyramids. The findings not only unveil the intrinsic characteristics of CBVO associated with its structure, but also highlight its potential as a NLO crystal.

Conflicts of interest

There are no conflicts to declare.

Acknowledgements

This work was financially supported by the National Key R&D Program of China (2021YFA0717800), National Natural Science Foundation of China (Grant No. 52002273 and 62104124), State Key Laboratory of Crystal Materials, Shandong University (No. KF2303).

References

1 P. S. Halasyamani and K. R. Poeppelmeier, Noncentro symmetric Oxides, *Chem. Mater.*, 1998, **10**, 2753–2769.
2 W. Zhang, X. Wang, G. Shen and D. Shen, Top-seeded growth, optical properties and theoretical studies of non-centrosymmetric $Te_2V_2O_9$, *Cryst. Res. Technol.*, 2012, **47**, 163–168.
3 Z. Lin, G. Wang and L. Zhang, Growth of a new nonlinear optical crystal $YCa_9(VO_4)_7$, *J. Cryst. Growth*, 2007, **304**, 233–235.
4 J. Olchowka, M. Colmont, H. Kabbour and O. Mentré, Bismuth and vanadate activators in $BiMVO_5$ (M = Ca, Mg,

Cd) phases: Structural, electronic and optical specificities, *J. Alloys Compd.*, 2017, **709**, 373–380.
5 Y. Kikukawa, K. Seto, S. Uchida, S. Kuwajima and Y. Hayashi, Solid-state umbrella-type inversion of a VO_5 square-pyramidal unit in a Bowl-type dodecavanadate induced by insertion and elimination of a guest molecule, *Angew. Chem., Int. Ed.*, 2018, **57**, 16051–16055.
6 A. Müller, R. Rohlfing, J. Döring and M. Penk, Formation of a Cluster Sheath around a Central Cluster by a "Self–Organization Process": the Mixed Valence Polyoxovanadate $[V_{34}O_{82}]^{10-}$, *Angew. Chem., Int. Ed. Engl.*, 1991, **30**, 588–590.
7 N. Zhuang, X. Liu, Q. Xu, X. Chen, B. Zhao, X. Hu and J. Chen, Crystal growth, nonlinear frequency-doubling and spectral characteristic of Nd: $Ca_9La(VO_4)_7$ crystal, *J. Alloys Compd.*, 2014, **595**, 113–119.
8 M. G. Johnston and W. T. Harrison, $Li(VO_2)_3(TeO_3)_2$, *Acta Crystallogr., Sect. C: Cryst. Struct. Commun.*, 2007, **63**, i57–i59.
9 J. Pan, Y. Li, Y. Cui, L. Zhao, X. Li and L. Han, Synthesis, crystal structure and nonlinear optical property of $Rb_3V_5O_{14}$, *J. Solid State Chem.*, 2010, **183**, 2759–2762.
10 T. Wu, X. Jiang, K. Duanmu, C. Wu, Z. Lin, Z. Huang, M. G. Humphrey and C. Zhang, Secondary-Bond-Driven Construction of a Polar Material Exhibiting Strong Broad-Spectrum Second-Harmonic Generation and Large Birefringence, *Angew. Chem., Int. Ed.*, 2023, e202318107.
11 Y. She, J. Jiao, Z. Wang, J. Chai, J. Song, N. Ye, Z. Hu, Y. Wu and C. Li, $LiVTeO_5$: A Mid-Infrared Nonlinear Optical Vanadium Tellurate Exhibiting Enhanced Second Harmonic Generation Activities and Notable Birefringence, *Inorg. Chem. Front.*, 2023, **10**, 6557–6565.
12 C. F. Sun, C. L. Hu, X. Xu, B. P. Yang and J. G. Mao, Explorations of new second-order nonlinear optical materials in the potassium vanadyl iodate system, *J. Am. Chem. Soc.*, 2011, **133**, 5561–5572.
13 P. S. Halasyamani, Asymmetric cation coordination in oxide materials: Influence of lone-pair cations on the intra-octahedral distortion in d^0 transition metals, *Chem. Mater.*, 2004, **16**, 3586–3592.
14 Z. Chen, Y. Liu, Y. Shi, W. Zhang, Q. Jing, Y. Fang and X. Dong, $M_3V_2B_{10}O_{23}$ (M = Ca, Sr): two new vanadoborates with $[V_2B_{10}O_{23}]($ double layers, *New J. Chem.*, 2017, **41**, 6730–6735.
15 Z. Chen, Z. Zhang, X. Dong, Y. Shi, Y. Liu and Q. Jing, Li_3VO_4: A Promising Mid-Infrared Nonlinear Optical Material with Large Laser Damage Threshold, *Cryst. Growth Des.*, 2017, **17**, 2792–2800.
16 J. Yeon, A. S. Sefat, T. T. Tran, P. S. Halasyamani and H. C. zur Loye, Crystal growth, structure, polarization, and magnetic properties of cesium vanadate, $Cs_2V_3O_8$: A structure-property study, *Inorg. Chem.*, 2013, **52**, 6179–6186.
17 J. Yeon, S. H. Kim and P. S. Halasyamani, $A_3V_5O_{14}$ (A = K^+, Rb^+, or Tl+), new polar oxides with a tetragonal tungsten bronze related structural topology: synthesis, structure, and functional properties, *Inorg. Chem.*, 2010, **49**, 6986–6993.
18 G. Han, Y. Wang, X. Su, Z. Yang and S. Pan, Growth, properties, and theoretical analysis of M_2LiVO_4 (M = Rb, Cs) crystals: two potential Mid-Infrared nonlinear optical materials, *Sci. Rep.*, 2017, **7**, 1901.
19 C. Wu, X. Jiang, L. Lin, Y. Hu, T. Wu, Z. Lin, Z. Huang, M. G. Humphrey and C. Zhang, A congruent-melting mid-infrared nonlinear optical vanadate exhibiting strong Second-Harmonic Generation, *Angew. Chem., Int. Ed.*, 2021, **60**, 22447–22453.
20 S. Chen, S. Pan, W. Zhao, H. Yu, H. Wu, Z. Yang and Y. Yang, A new noncentrosymmetric vanadoborate: synthesis, crystal structure and characterization of $K_2SrVB_5O_{12}$, *Dalton Trans.*, 2012, **41**, 9202–9208.
21 X. Fan, S. Pan, X. Hou, X. Tian, J. Han, J. Haag and K. R. Poeppelmeier, Growth and properties of single crystals of noncentrosymmetric $Na_3VO_2B_6O_{11}$, *Cryst. Growth Des.*, 2010, **10**, 252–256.
22 V. V. Titkov, S. Y. Stefanovich, D. V. Deyneko, Y. Y. Dikhtyar, S. M. Aksenov, O. V. Baryshnikova, A. A. Belik and B. I. Lazoryak, Isovalent and aliovalent cation substitutions in the anion sublattice of whitlockite-type ferroelectrics $Ca_9RE(VO_4)_7$ with RE = Y and Yb, *J. Solid State Chem.*, 2019, **279**, 120966.
23 A. K. Paidi, P. W. Jaschin, K. B. R. Varma and K. Vidyasagar, Syntheses and Characterization of $AM_2V_2O_{11}$ (A = Ba, Sr, Pb; M = Nb, Ta) Vanadates with Centrosymmetric and Noncentrosymmetric Structures, *Inorg. Chem.*, 2017, **56**, 12631–12640.
24 H. X. Tang, Y. X. Zhang, C. Zhuo, R. B. Fu, H. Lin, Z. J. Ma and X. T. Wu, A niobium oxyiodate sulfate with a strong second-harmonic-generation response built by rational multi-component design, *Angew. Chem., Int. Ed.*, 2019, **58**, 3824–3828.
25 H. Jiang, S. Huang, Y. Fan, J.-G. Mao and W. Cheng, Explorations of New Types of Second-Order Nonlinear Optical Materials in Cd(Zn)-VV-TeIV-O Systems, *Chem. – Eur. J.*, 2008, **14**, 1972–1981.
26 M. Xia, X. Jiang, Z. Lin and R. Lit, "All-Three-in-One": A New Bismuth-Tellurium-Borate Bi_3TeBO_9 Exhibiting Strong Second Harmonic Generation Response, *J. Am. Chem. Soc.*, 2016, **138**, 14190–14193.
27 Q. Liu, Q. Wu, T. Wang, L. Kang, Z. Lin, Y. Wang and M. Xia, Polymorphism of $LiCdBO_3$: Crystal structures, phase transitions and optical characterizations, *Chin. J. Strut. Chem.*, 2023, **42**, 100026.
28 I. Radosavljevic, J. A. Howard and A. W. Sleight, Synthesis and structure of two new bismuth cadmium vanadates, $BiCdVO_5$ and $BiCd_2VO_6$, and structures of $BiCa_2AsO_6$ and $BiMg_2PO_6$, *Int. J. Inorg. Mater.*, 2000, **2**, 543–550.
29 J. W. Steed, Should solid-state molecular packing have to obey the rules of crystallographic symmetry?, *CrystEngComm*, 2003, **5**, 169–179.
30 G. M. Sheldrick, A short history of SHELX, *Acta Crystallogr., Sect. A: Found. Crystallogr.*, 2008, **64**, 112–122.
31 P. Negrier, M. Barrio, J. L. Tamarit, N. Veglio and D. Mondieig, Structure of Phase III and Polymorphism of $(CH_3)_3CBr$, *Cryst. Growth Des.*, 2010, **10**, 2793–2800.
32 J. Tauc, Absorption edge and internal electric fields in amorphous semiconductors, *Mater. Res. Bull.*, 1970, **5**, 721–729.

33 S. K. Kurtz and T. T. Perry, A powder technique for the evaluation of nonlinear optical materials, *J. Appl. Phys.*, 1968, **39**, 3798–3813.
34 J. Jiao, C. Li, Y. She, N. Ye, Z. Hu and Y. Wu, Achieving broadband ultraviolet to mid-infrared transparency in germanate-based nonlinear optical crystals $Cs_3REGe_3O_9$ (RE = Y, Gd), *Inorg. Chem. Front.*, 2023, **10**, 6869–6878.
35 J. P. Perdew, A. Ruzsinszky, G. I. Csonka, O. A. Vydrov, G. E. Scuseria, L. A. Constantin, X. Zhou and K. Burke, Restoring the density-gradient expansion for exchange in solids and surfaces, *Phys. Rev. Lett.*, 2008, **100**, 136406.
36 S. J. Clark, M. D. Segall, C. J. Pickard, P. J. Hasnip, M. I. Probert, K. Refson and M. C. Payne, First principles methods using CASTEP, *Z. Kristallogr. – Cryst. Mater.*, 2005, **220**, 567–570.
37 D. Vanderbilt, Soft self-consistent pseudopotentials in a generalized eigenvalue formalism, *Phys. Rev. B: Condens. Matter Mater. Phys.*, 1990, **41**, 7892.
38 J. P. Perdew, K. Burke and M. Ernzerhof, Generalized gradient approximation made simple, *Phys. Rev. Lett.*, 1996, **77**, 3865.
39 W. Zhao, J. Jiao, Y. She, F. Liang, N. Ye, Z. Hu, Y. Wu and C. Li, Tailored Ordered Structures with Functional Units of Distorted $[NbO_6]$ and Antiparallel $[GeO_4]$ for Enhanced Birefringence in Germanate Crystal, *Adv. Opt. Mater.*, 2022, **10**, 2201704.
40 L. G. DeShazer, Improved midinfrared polarizers using yttrium vanadate, *Proc. SPIE*, 2002, **4481**, 10–16.
41 C. Z. Bi, J. Y. Ma, J. Yan, X. Fang, D. Z. Yao, B. R. Zhao and X. G. Qiu, Far-infrared optical properties of YVO_4 single crystal, *Eur. Phys. J. B*, 2006, **51**, 167–171.
42 N. Amdouni, H. Zarrouk and C. M. Julien, Synthesis, structure and intercalation of brannerite $LiWVO_6$ wet-chemical products, *J. Mater. Sci.*, 2003, **38**, 4573–4579.
43 G. Busca, G. Ricchiardi, D. S. H. Sam and J.-C. Volta, Spectroscopic characterization of magnesium vanadate catalysts. Part 1.—Vibrational characterization of $Mg_3(VO_4)_2$, $Mg_2V_2O_7$ and MgV_2O_6 powders, *J. Chem. Soc., Faraday Trans.*, 1994, **90**, 1161–1170.
44 G. Busca, Differentiation of mono-oxo and polyoxo and of monomeric and polymeric vanadate, molybdate and tungstate species in metal oxide catalysts by IR and Raman spectroscopy, *J. Raman Spectrosc.*, 2002, **33**, 348–358.
45 T. Sivakumar, K. M. Ok and P. S. Halasyamani, Synthesis, structure, and characterization of novel two- and three-dimensional vanadates: $Ba_{2.5}(VO_2)_3(SeO_3)_4{\cdot}H_2O$ and $La(VO_2)_3(TeO_6){\cdot}3H_2O$, *Inorg. Chem.*, 2006, **45**, 3602–3605.
46 A. Ciupa-Litwa, J. A. Zienkiewicz, M. Stefanski, M. Ptak, A. Majchrowski and M. Chrunik, Vibrational and optical studies of a nonlinear optical crystal, $Cs_2Bi_2O(Ge_2O_7)$, *Spectrochim. Acta, Part A*, 2021, **259**, 119816.
47 S. Xue, H. He, Q. Fan, C. Yu, K. Yang, W. Huang, Y. Zhou and Y. Xie, La/Ce-codoped Bi_2O_3 composite photocatalysts with high photocatalytic performance in removal of high concentration dye, *J. Environ. Sci.*, 2017, **60**, 70–77.
48 X. Su, Y. Chu, Z. Yang, B.-H. Lei, C. Cao, Y. Wang, Q. Liu and S. Pan, Intense d-p Hybridization Induced a Vast SHG Response Disparity between Tetrahedral Vanadates and Arsenates, *J. Phys. Chem. C*, 2020, **124**, 24949–24956.
49 W. Chen, W. Zhang, M. H. Lee, Q. Jing, X. Lu and Z. Chen, $BaV_2O_6{\cdot}H_2O$: A nonlinear optical crystal with a large bandgap, *Opt. Mater.*, 2019, **88**, 642–647.
50 X. Dong, H. Huang, L. Huang, Y. Zhou, B. Zhang, H. Zeng, Z. Lin and G. Zou, Unearthing Superior Inorganic UV Second-Order Nonlinear Optical Materials: A Mineral-Inspired Method Integrating First-Principles High-Throughput Screening and Crystal Engineering, *Angew. Chem., Int. Ed.*, 2024, e202318976.